Axisymmetric Sonic Flow Computed by a Numerical Method Applied to Slender Bodies

Y. C.-J. SEDIN*
SAAB-SCANIA AB, Linköping, Sweden

The present method is based on a decomposition of the velocity potential into two new functions. These two functions, forming a new system, can be stably integrated in opposite radial directions. A far-field boundary condition in free air is established at a finite radius by means of the asymptotic Guderley far-field expansion. Porous wind tunnel walls also can be handled by this method. A pronounced feature of this iterative method, considering only one new function at a time, is a rather high rate of convergence. The agreement with experimental data and other comparable methods is found to be very good.

I. Introduction

THE transonic flight regime characterized by mixed subsonic and supersonic flow has gained a renewed interest during the last years. The problem of designing an aircraft which could be economically operated at Mach numbers close to unity has considerably spured the research efforts. Axisymmetric flow, however, still plays a rather central role to the engineer when deciding upon a suitable cross-sectional area distribution. The theoretical basis for this is the transonic area rule of Whitcomb,[1] and Oswatitsch and Keune.[2] This equivalence rule has recently been extended and investigated in detail by Cheng and Hafez,[3] which illustrate the importance of axisymmetric flow at near sonic speed.

The present numerical method, here applied to axisymmetric bodies at sonic speed, was originally suggested by Berndt.[4] The idea is to generalize the slender-body behavior close to the body to decompose the velocity potential into two new functions. A differential system of two coupled equations is then formed. If the equations for the two functions are regarded one at a time, assuming the other function to be known, the system can be temporarily interpreted as two parabolic equations. The time-like variables for the two equations are defined in opposite radial directions.

The intension is to alternatingly integrate the two equations iteratively outwards and inwards, using the body boundary condition as initial values for one of the functions and the Guderley[5] far-field expansion as initial data for the other function. A porous wall can also be applied as an outer condition. The approach of using the Guderley[5] expansion as a far field condition in free air has earlier been applied by Yoshihara.[6] The present technique however determines several far-field parameters every new cycle during the course of iteration. Recently, Euvrard and Tournemine[16] presented a method where they used the corresponding two-dimensional far-field analogy as an outer condition.

This paper is an extension of earlier work presented by Berndt and Sedin.[4,7] It covers a number of bodies and flowfields computed from far upstream down to the limiting characteristic in free air. A wind-tunnel wall interference case has also been computed in order to check out the discrepancies between calculations and experimental data. The required number of full-cycle iterations to and fro was about 5–10 for a free-air case while a wind-tunnel case needed about 10–20 cycles.

Presented as Paper 74-544 at the AIAA 7th Fluid and Plasma Dynamics Conference, Palo Alto, Calif., June 17–19, 1974; submitted July 10, 1974; revision received October 11, 1974. The author wishes to acknowledge S. B. Berndt of the Royal Institute of Technology in Stockholm who suggested the subject and in many respects made this work possible. Several calculations in the paper were performed by R. Mattsson and J. Anderson at the above institute.
Index categories: Subsonic and Transonic Flow; Aircraft Aerodynamics (Including Component Aerodynamics).
* Aerodynamic Research Engineer. Member AIAA.

II. Axisymmetric Sonic Flow

A. Basic Equations

Suppose that the flowfield around the slender body as pictured in Fig. 1 can be described by the velocity potential ϕ. The velocity field is then given by $\boldsymbol{v} = \text{grad}\,\phi$.

The problem for ϕ is formulated by means of the continuity and energy equations as follows:

$$(a^2-\phi_{x'}{}^2)\phi_{x'x'}+(a^2-\phi_{r'}{}^2)\phi_{r'r'}+(a^2/r')\phi_{r'}-2\phi_{x'}\phi_{r'}\phi_{x'r'}=0 \tag{1a}$$

$$a^2 = a_\infty{}^2-[(\gamma-1)/2](\phi_{x'}{}^2+\phi_{r'}{}^2-1)$$

The boundary conditions are

$$r' \to r'_B(x'): \quad \phi_{r'}/\phi_{x'} = (dr'_B/dx') \tag{1b}$$
$$(x'^2+r'^2) \to \infty: \quad \phi \to x'$$

In the case of a porous wind-tunnel wall the outer condition of Eq. (1b) is exchanged and approximately simulated by

$$r' \to r'_w: \quad \phi_{r'}+P(\phi_{x'}-1)=0 \tag{1c}$$

P is the porosity coefficient of the wall.

The first-order outer problem is now established by introducing a perturbation potential φ and expanding ϕ and φ along a convenient body slenderness parameter $\tau \ll 1$. The space variables are normalized with the unit of length c.

$$\phi = c[x+\tau^2\varphi(x,\eta;\tau)]$$
$$x = x'/c; \quad \eta = \tau(1+\gamma)^{1/2}r'/c \tag{2}$$
$$s = \tfrac{1}{2}(r'_B/c)^2\cdot\tau^{-2}$$

It is supposed that the body radius function $r'_B(x')$ is of order τ so that the normalized cross-sectional area s is of order unity

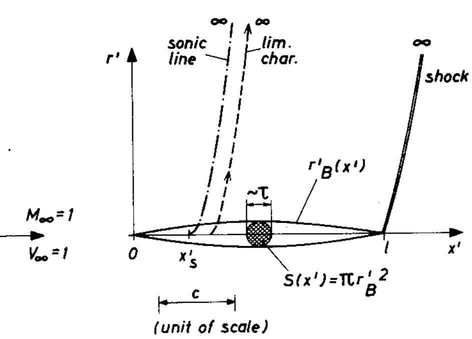

Fig. 1 Axisymmetric body.

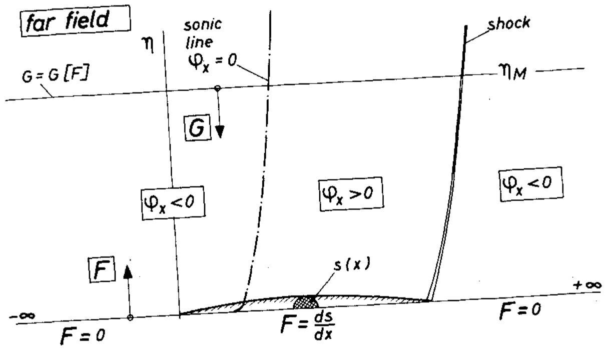

Fig. 2 Integration pattern.

in the limit $\tau \to 0$. Inserting the expansion equation (2) into Eq. (1a) gives the outer problem to the first-order

$$\varphi_{\eta\eta} + (1/\eta)\varphi_\eta = \varphi_x \varphi_{xx} \tag{3a}$$

The first-order inner solution of Eq. (1a) is in principle given by neglecting the right-hand side of Eq. (3a). Upon doing so the left-hand side of Eq. (3a) can be integrated easily and a logarithm $\ln \eta$ will appear in the solution. Thus in the inner limit, $\eta \to 0$, the potential φ $(x, \eta; \tau)$ must have a logarithmic line singularity. The strength of this singularity is determined by the body boundary condition of Eq. (1b).

Hence in the inner limit the following condition must be fulfilled by the outer solution

$$\eta \to 0: \quad \eta\varphi_\eta = (ds/dx) \tag{3b}$$

The inner slender-body solution, which obviously is included in the outer, Eqs. (3a) and (3b), is as follows:

$$\varphi \approx (ds/dx)\ln \eta + g(x) \tag{4}$$

This simple solution breaks down at infinity so the unknown function $g(x)$ must be determined by matching to an outer solution, which satisfies the condition at infinity. Using the approximation (4) the pressure coefficient C_p is expressible along the body surface as follows:

$$C_p = -2\tau^2\left(\frac{d^2s}{dx^2}\ln \eta_B + \frac{1}{4}\left(\frac{ds}{dx}\right)^2 \Big/ s + \frac{dg}{dx}\right)$$
$$\eta_B = \tau^2[2(\gamma+1)s]^{1/2} \tag{5}$$

In essence, a generalization of the slender-body approximation (4) is the very basis of the present numerical method, which will be described in Sec. IIB.

B. The Present Method of Solution

Summarizing Sec. IIA, the following problem is at hand. The equation to be solved for φ is that given by Eq. (3a). The inner boundary condition is stated by Eq. (3b). The outer condition is expressed by one of the relations below:

a) Free air

$$(x^2+\eta^2) \to \infty, \quad \varphi \to 0 \tag{3c}$$

b) Porous wall

$$\eta \to \eta_w, \quad (\varphi_\eta + p\varphi_x) = 0 \tag{3d}$$

The inner slender-body behavior of Eq. (3a) is to the first approximation found in relation (4). The structure of this simple solution is going to be retained in a more generalized solution by introducing two new functions F and G in the following manner

$$F = \eta\varphi_\eta$$
$$G = \varphi - \eta\varphi_\eta \ln(\eta/\eta_M) \tag{6}$$

F and G are functions of both x and η. The symbol η_M denotes a fixed outer matching radius. By means of Eq. (3a) and the definition Eq. (6), a new coupled system for F and G can be established as follows:

$$F_\eta = \eta U(\ln(\eta/\eta_M)F_{xx} + G_{xx})$$
$$G_\eta = -\eta \ln(\eta/\eta_M)U(G_{xx} + \ln(\eta/\eta_M)F_{xx}) \tag{7}$$

The letter U stands for the perturbation velocity φ_x expressible in F_x and G_x by relation (6).

The intention now is to numerically integrate the functions F and G in opposite radial directions between $\eta = 0$ and $\eta = \eta_M$ as indicated in Fig. 2. Initial values for F are then supposed to be given by the body boundary condition, $F = (ds/dx)$, along the axis $\eta = 0$. Initial values for G are imposed by some convenient far-field or wall-condition, $G = G[F]$, along the outer boundary η_M.

The original potential Eq. (3a) is of a mixed elliptic-hyperbolic type depending on the sign of φ_x. If the equations for F and G are regarded separately, assuming the other function to be known, the system Eq. (7) can be temporarily interpreted as two parabolic equations. The two time-like directions are then in opposite radial directions.

In the subsonic domain the parabolic time-like directions are compatible with those naturally suggested by the body and far-field boundary values. In the supersonic region however these stable time-like directions are reversed calling for some special treatment to keep the same integration pattern as in the subsonic domain. Numerically this has been done in two different ways. The first approach is the method of characteristics. The second tried method is a straightforward finite difference scheme, which not violates the hyperbolic region of dependence for the original Eq. (3a) when applying the x-differentials.

An iterative method is formed by repeatedly solving the F and G-functions one at a time outwards and inwards with an inner condition close to the axis $\eta = 0$ and an outer condition applied at a finite radius $\eta = \eta_M$. The outer condition consists of a Guderley[5] far-field expansion or a porous wall description. Appropriate side conditions also have to be imposed. Initial values for G along $\eta = \eta_M$ are evaluated at each new iteration cycle by fitting the streamline slope to the newly computed values of F at the matching radius η_M. This is represented by the functional symbol $G = G[F]$ in Fig. 2. This involves either the calculation of new far-field parameters or alternatively an integration of the porous wall condition, Eq. (3d).

C. The Guderley Far-Field Expansion

A basic far-field solution of the potential Eq. (3a) was originally demonstrated by Guderley,[5] and Guderley-Yoshihara.[8] This solution, as shown below, is an exact self-similar integral of Eq. (3a). It describes the asymptotic behavior of the flow at large distances from a body in a sonic freestream.

$$\varphi = C^3\eta^{-2/7}f(z)$$
$$z = C^{-1}(x - x_o)\eta^{-4/7} \tag{8}$$

The solution depends on two parameters, C and x_o, and is strongly singular at $x = x_o$, $\eta = 0$. The parameters C and x_o are a priori unknown and in some way related to the geometry of the body.

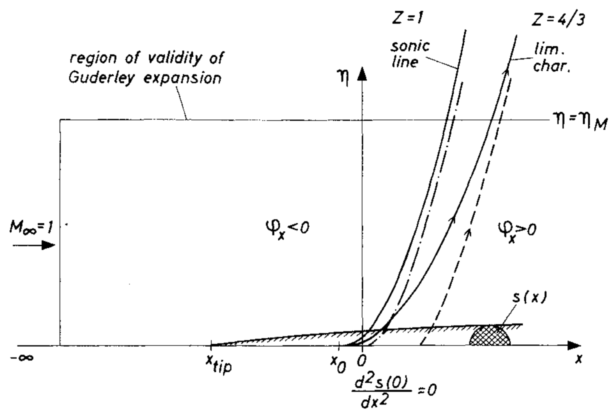

Fig. 3 Guderley solution.

The fitting in of the basic solution is sketched in Fig. 3. The parabola $z = 1$ is the sonic line ($\varphi_x = 0$) and $z = \frac{4}{3}$ represents the limiting characteristic, which is the last outgoing machline that intersects the sonic line. The dashed lines are assumed to be the true solution including the proper near field.

For the time being the flow upstream of the limiting characteristic has been considered only, though the solution, Eq. (8), is capable of describing a shock wave. However, downstream of the limiting machline the flow is of a pure supersonic nature partly reducing the interest in this area.

The singularity of Eq. (8) prevents it from being used all the way down to the body. To get as close as possible however and have the possibility of smoothly fitting in the far-field to the near-field, it is feasible to expand the far-field around the solution, Eq. (8).

$$\varphi = C^3\left[\eta^{-2/7}f(z) + \sum_{j=1}^{\infty} \alpha_j \eta^{\nu_j} g_j(z)\right] \tag{9}$$

The functions g_j are solutions of a linear perturbation problem around the basic solution and the exponents ν_j are the corresponding eigenvalues. The number of parameters to be determined have now been increased with an infinite set of constants α_j. The first two terms g_1 and g_2 are linear perturbations of the basic solution with respect to C and x_o. Hence the coefficients α_1 and α_2 can be exchanged for small corrections in C and x_o instead. Analytical descriptions of expansion, Eq. (9), have been obtained independently by several authors. A literature survey can be found in Ref. 4. The approach of Randall[9] is followed here.

From the slender-body approximation, Eq. (4), it follows that the isovelocity line $\varphi_x = 0$, not quite the sonic line in the inner limit, asymptotically approaches the x axis at that x-station where $d^2s/dx^2 = 0$. From this point of view it is convenient to place the origin $x = 0$ at this x-station and to define the unit of length c by the formula

$$c = S(x_s')/(dS(x_s')/dx'); \quad d^2S(x_s')/dx'^2 = 0 \tag{10a}$$

$S = \pi r_B'^2$ is the dimensional cross-sectional area and x' belongs to the dimensional frame shown in Fig. 1. The corresponding slenderness parameter τ is chosen to be

$$\tau = [S(x_s')/2\pi]^{1/2}/c \tag{10b}$$

From this geometrical normalization, where $x = 0$ corresponds to x_s', it follows for arbitrary bodies that

$$s(0) = (ds(0)/dx) = 1; \quad (d^2s(0)/dx^2) = 0 \tag{10c}$$

This normalization was suggested by Berndt in Ref. 4.

To use the Guderley expansion as an outer condition, it is necessary to estimate the region of validity of the asymptotic solution. An approach to this problem has been made by Berndt.[4] More specifically the following result was obtained:[4] $\eta_M = 0.762$; $C = 0.787$; $x_o = -0.431$. It should here be stressed that this estimation is only a crude ordering.

III. Numerical Procedures

A. The Free Air Case

Only the true transonic region upstream of the limiting characteristic is to be considered. The Guderley far-field expansion is supposed to be valid outside and on the boundary $ABCH$ of Fig. 4. The problem for φ, stated by Eq. (3a) with boundary conditions (3b) and (3c), is solved numerically by integrating system (7) in the subsonic region $ABCO$ and applying the method of characteristics in the supersonic domain $OCHE$. In brief, the following iteration scheme can be outlined with notations from Fig. 4.

a) Guess an initial sonic line OC and a small number of far-field parameters. Make a plausible estimate of the G field by aid of the Guderley expansion. Guess the start position E of the limiting characteristic. Compute the supersonic domain $OCDE$ by the method of characteristics.

b) Perform the F integration from $\eta = 0$ to $\eta = \eta_M$ with initial values given by condition (3b).

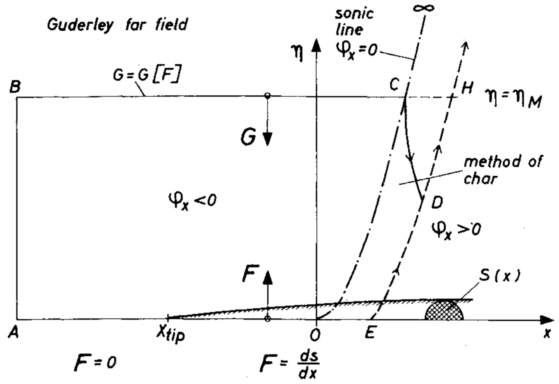

Fig. 4 Regions of integration, free air.

c) Solve for new far-field parameters by fitting the streamline slope of the Guderley expansion to the slope obtained in b) along $\eta = \eta_M$.

d) Perform the G integration from $\eta = \eta_M$ to $\eta = 0$ with initial data, $G = G[F(x, \eta_M)]$, calculated in c). Trace successively a new path of the sonic line OC ($\varphi_x = 0$) by streamwise sweeping the G integration at every new "time-level."

e) Compute the supersonic region by the method of characteristics with a corrected start point E for the limiting characteristic.

f) Check the solution. If not good enough return to b) and continue another full-cycle iteration.

The integration of F and G in system Eq. (7), is carried out in a rectangular mesh net equidistant in x and $\ln \eta$. Mixed explicit and implicit schemes are used with central-differences simulating the x derivatives. For the F equation the side condition along AB consists of imposing the gradient F_x obtained from the Guderley expansion. The side condition for the F-integration along the sonic line ($\varphi_x = 0$) OC is established by requiring continuity in both F and F_x, which are calculated by the method of characteristics. Giving both F and F_x along OC is in principle the same condition when OC is a true sonic line.

Regarding the G integration the boundary condition along AB is made up of G_x evaluated by the Guderley expansion of φ_x inserted into relation, Eq. (6). No conditions at all are imposed along the line OC. A new sonic line is traced by successively sweeping every radial "time-level" streamwise until the line $\varphi_x = 0$ is found.

The method of characteristics is mainly carried out in the same way as described in Ref. 7. Numerically the method is worked out by discretizing the following equations along the two families of characteristics:

$$dF/d(U^{3/2}) = \pm(2/3)e^q$$
$$dx/d(U^{3/2}) = \pm(2/3)e^q(dq/dU) \tag{11}$$
$$F = \eta\varphi_\eta; \quad U = \varphi_x; \quad q = \ln \eta$$

Boundary conditions are applied along OC ($U = 0$) and at the axis $\eta = 0$ ($F = ds/dx$). To calculate the region CHD the velocity U is assigned along CH by means of the far-field. The numerical model of Eq. (11) can easily be shown to have the right analytical behavior close to the sonic line $U = 0$.

In practice the boundary condition at the x-axis ($\eta = 0$, Fig. 4) is displaced to a small radius outside the axis to avoid the logarithmic singularity of U. This is also the case when integrating system, Eq. (7).

The calculations of the far-field parameters C, x_o, and α_j are based on a least square fit of the Guderley expansion for F to computed near-field values of F obtained along BC and the characteristic line CD. Two more conditions are also imposed, namely a streamline displacement condition at B and a velocity condition at D. The problem of solving the far-field is linear in α_j but nonlinear in C and x_o. Hence the problem is evaluated by iteration keeping C and x_o fixed and successively correcting C and x_o with α_1 and α_2. The number of perturbation terms used in the Guderley expansion has usually been 6–8.

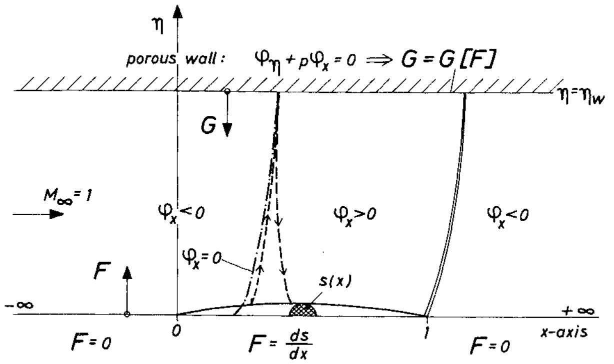

Fig. 5 Wall interference.

B. The Wall Interference Case

In this case the whole flowfield between the x-axis ($\eta = 0$, Fig. 5) and the tunnel wall is considered from upstream infinity to downstream infinity. A simplification is here introduced by integrating the decomposed system, Eq. (7), in the same rectangular mesh net in both the subsonic and supersonic domains. Hence the somewhat laborious method of characteristics is abandoned.

The problem for φ is formulated by Eq. (3a) with boundary conditions, Eqs. (3b) and (3d). The unit of length is equal to the length of the body, which is set equal to unity according to Fig. 5. The slenderness parameter τ is here defined as the diameter-length ratio of the body.

Numerically the problem is solved by integrating system, Eq. (7), in both the subsonic ($\varphi_x < 0$) and supersonic ($\varphi_x > 0$) regions. The natural directions of integration are chosen to be those of the subsonic domain. Problems may be expected in the supersonic region where the stable "time-like" directions are reversed from the "parabolic" point of view (see Sec. IIB). However to maintain the same integration pattern in the supersonic flow the difficulties are avoided by taking backward differences with regard to x. With this move the hyperbolic region of dependence for the original potential, Eq. (3a), is not violated when concerning the x derivatives. The adopted differential schemes are examplified in Fig. 6.

An iterative procedure is formed by alternatingly integrating the F and G functions outwards and inwards in a reciprocating manner. Initial values are applied close to the body axis, ($F = ds/dx$), and at the wall radius, ($G = G[F]$). The wall condition implies a successively corrected $G = G[F]$ along the wall by integrating the wall condition, Eq. (3d), after every completed F-integration. The whole process is started up by initially assuming the G field to be zero. The appropriate side conditions at infinity are easily fulfilled by mapping the x-axis ($\eta = 0$, Fig. 5) on to a finite interval.

Mixed implicit and explicit schemes are used in the subsonic domain with central differences (with regard to x) as shown in

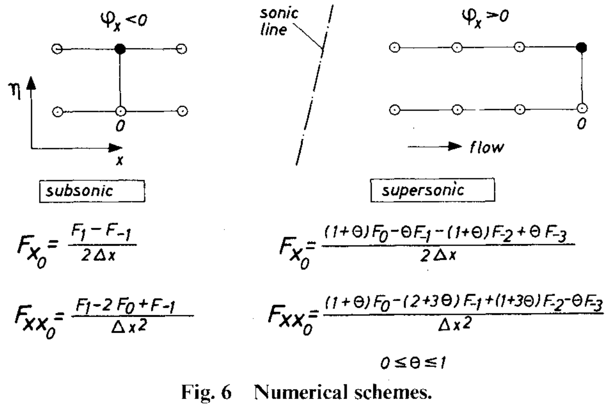

Fig. 6 Numerical schemes.

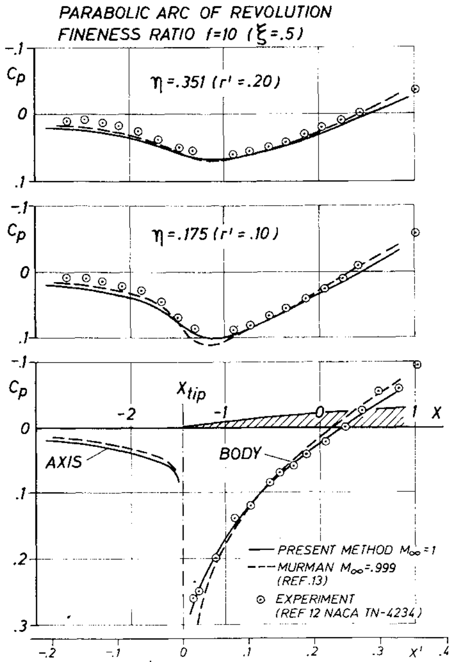

Fig. 7 Pressure distribution of a parabolic arc.

Fig. 6. The supersonic scheme is explicit only and utilizes backward-differences equal to those originally applied by Murman and Cole.[10] Every radial "time-level" is always swept streamwise in order to capture an appearing shock wave. In the supersonic domain mixed first- and second-order accuracy schemes are used to add dissipation into the system.

IV. Results

A. Comparison with Experiment and Other Methods of Computation

Three bodies of the generalized parabola family given in Ref. 11 have been treated. The bodies are characterized by an exponent n related to the relative position ξ of the maximum thickness location. Some geometrical properties are given in Table 1 according to the normalization chosen in Sec. IIC for the free-air case. The fineness ratio f is the length-diameter ratio while τ is defined by relation, Eq. (10b).

Table 1 Bodies considered

ξ	n	f	τ	x_{tip}	$\frac{d^2s(tip)}{dx^2}$	$\frac{d^3s(0)}{dx^3}$
0.3	6.03	12	0.271	−1.42	1.75	−0.61
0.5	2.0	10	0.163	−1.46	1.50	−0.75
0.7	6.03	12	0.086	−1.75	0.69	−1.93

Figures 7–9 show computed pressure distributions for the bodies of Table 1 in the free air case. The agreement with experimental data taken from McDevitt and Taylor[11,12] is found to be quite satisfactory. Some discrepancies however are found, especially far upstream, which is clearly demonstrated in Fig. 7. This disagreement can probably be blamed on wind-tunnel wall interference, which seems to be verified by the computed porous wall case of Fig. 10.

A comparison with other methods of computation is illustrated in Figs. 7 and 9 for the free air case and in Fig. 11 for the porous wall case. The parabolic arc body ($\xi = 0.5$, $n = 2$) of Fig. 7 is compared with calculations made by Murman[13,14] at Mach number 0.999. Generally the agreement is very good

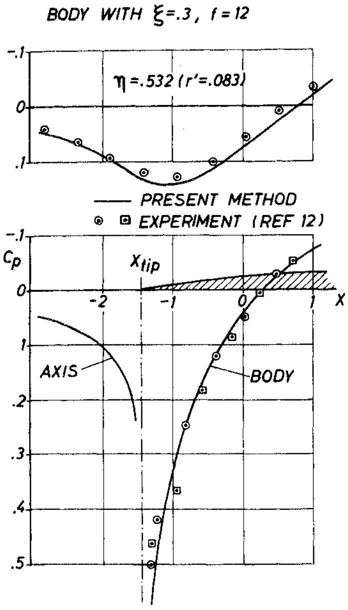

Fig. 8 Pressure distribution of a body with $\xi = 0.3$.

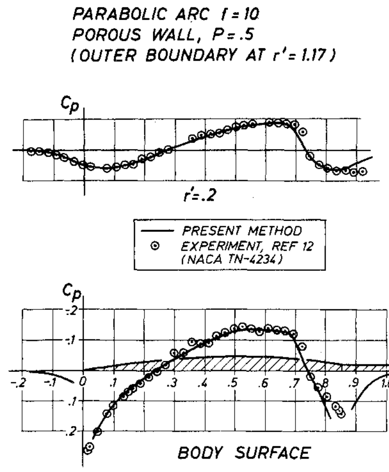

Fig. 10 Parabolic arc inserted into a porous wind tunnel.

apart from slightly different pressure gradients. If these discrepancies are due to the different methods of computation or the fact that Murman used a subsonic far-field is hard to say without a more detailed investigation.

In Fig. 9 a comparison is made between the present method and the local linearization method of Spreiter and Alksne.[15] The results are in a satisfactory agreement though slightly different trends are obtained for this body with $\xi = 0.7$, $n = 6.03$. Some typical results concerning the Guderley expansion are found in Table 2 for three different bodies. Values are shown of the first four perturbation terms among which the third is the dominating part.

Generally it is interesting to see how the parameter C is of about the same order and that x_o is close to the point where $(d^2s/dx^2) = 0$ for all the bodies. More details about the Guderley expansion of a parabolic arc ($\xi = 0.5$) can be found in Sec. IVB.

An attempt to compute the wall interference effects for a parabolic arc body in the NASA Ames 14-ft tunnel is illustrated in Fig. 10. The length of the body is here chosen as the unit of scale. The porosity parameter P is equal to 0.5 and the equivalent tunnel radius is $r' = 1.17$. The agreement with experimental data is very good. The definition of P is the same as that used by Bailey.[16] A comparison between the present method and com-

Table 2 Far-field parameters

ξ	0.3	0.5	0.7
C	0.8278	0.8213	0.7958
x_o	0.0360	−0.0637	−0.2620
α_1	0.0002	−0.0003	−0.0001
α_2	−0.0004	0.0007	0.0002
α_3	−1.3143	−1.0612	−0.5576
α_4	−0.7070	−0.5630	−0.0932

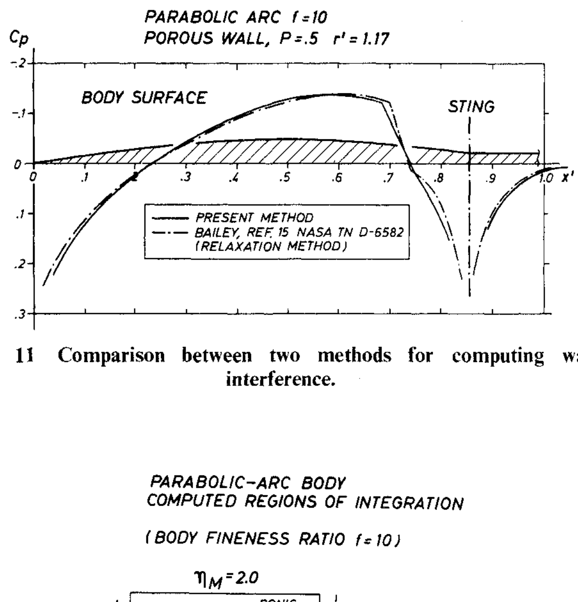

Fig. 11 Comparison between two methods for computing wall interference.

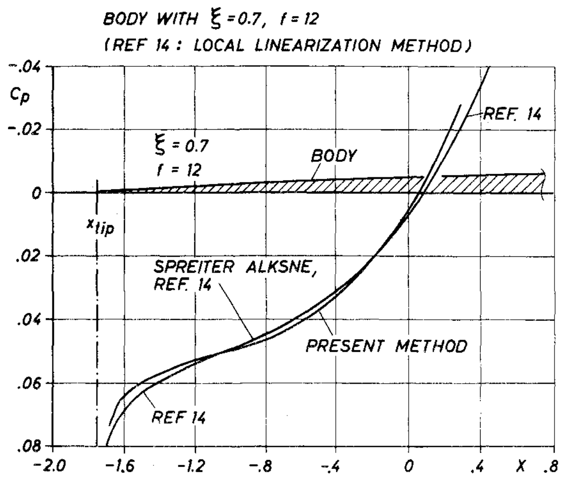

Fig. 9 Surface pressure distribution of a body with $\xi = 0.7$.

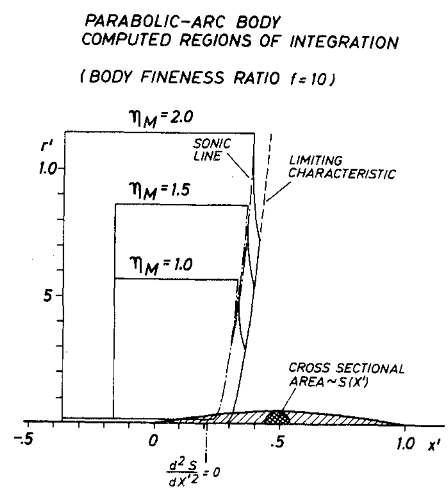

Fig. 12 Variations of the far-field boundary.

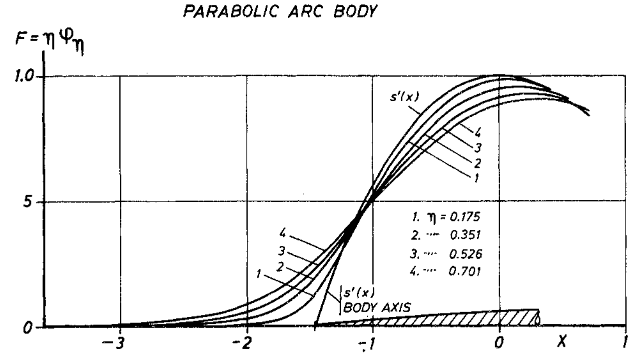

Fig. 13 Radial velocity distribution $F = \eta\varphi_\eta$.

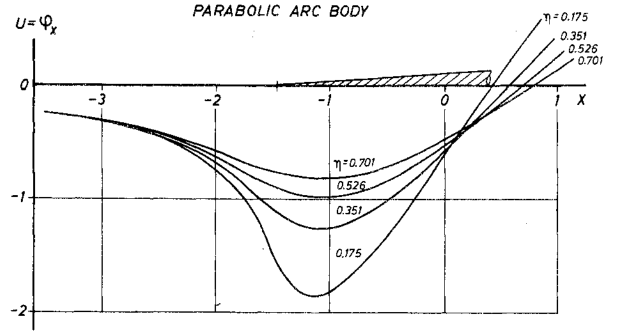

Fig. 15 Axial velocity distribution $U = \varphi_x$.

putations made by Bailey[16] is shown in Fig. 11. The agreement between the two methods is excellent apart from some deviations locally around the shock. These discrepancies are probably because the present method has been applied with a larger mesh size in x.

B. The Flow Structure Around a Parabolic Arc Body

Some detailed studies of the flow around the forward part of a parabolic arc body ($\xi = 0.5$, $n = 2$) in a sonic freestream will be displayed. Both the near-field and the far-field have been investigated for three different regions of integration, as depicted in Fig. 12.

Figures 13–15 give the overall view of the near-field at four radii. These radii are $\eta = 0.175, 0.351, 0.526, 0.701$, which correspond to $r' = 0.1, 0.2, 0.3, 0.4$ for a body of fineness ratio $f = 10$. The outer matching radius is placed at $\eta_M = 2.0$. Figure 13 shows that the slender-body approximation, Eq. (4), is most confined to regions where $\varphi_x \varphi_{xx}$ of Eq. (3a) is small. This is the case along the line of zero acceleration outside the nose-tip and at the sonic line.

The influence from the nose-tip singularity is most sensitively illustrated in Fig. 14. In practice the nose-tip singularity is of limited importance due to the logarithm of the composition, Eq. (6). The logarithmic term heavily dominates the pressure close to the body. In fact it is only necessary to estimate a decent value of g_x at $x = 0$ to get a rather good surface pressure, Eq. (5), upstream of $x = 0$. This is probably one of the secrets behind the remarkable accuracy of the local linearization method.[15]

An investigation of the Guderley expansion and its dependence on the outer matching radius has been performed and some of the results are shown in Figs. 16–18. The tested matching radii are $\eta_M = 1.0, 1.5, 2.0$ and these values are illustrated in Fig. 12 for a body with $f = 10$. The following typical values of the far-field parameters have been obtained with six perturbation terms.

Table 3 Variations of the far-field boundary

η_M	1.0	1.5	2.0
C	0.8165	0.8202	0.8213
x_o	−0.1096	−0.0873	−0.0637
α_1	−0.0012	0.0190	−0.0003
α_2	0.0033	0.0209	0.0007
α_3	−0.8843	−0.9729	−1.0612
α_4	−0.3338	−0.5521	−0.5630
α_5	−0.3169	−0.2673	−0.6163
α_6	−0.1599	−0.2561	−0.0469

It is interesting to note that C and x_o are rather unaffected by changes in η_M and that x_o is close to the point where $(d^2s/dx^2) = 0$. The dominating perturbation contribution corresponds to the coefficient α_3.

Three typical sonic lines ($\varphi_x = 0$) can be seen in Fig. 16. The two cases with $\eta_M = 1.5, 2.0$ agree fairly well, even with respect to the far-field. All three cases, however, seem to tend to the

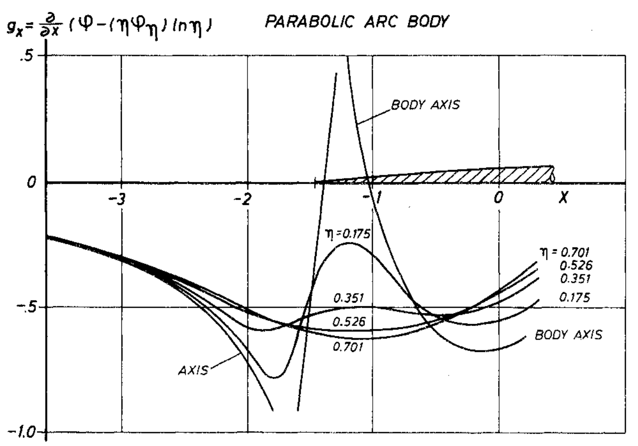

Fig. 14 Distribution of $g_x = \varphi_x - F_x \ln \eta$.

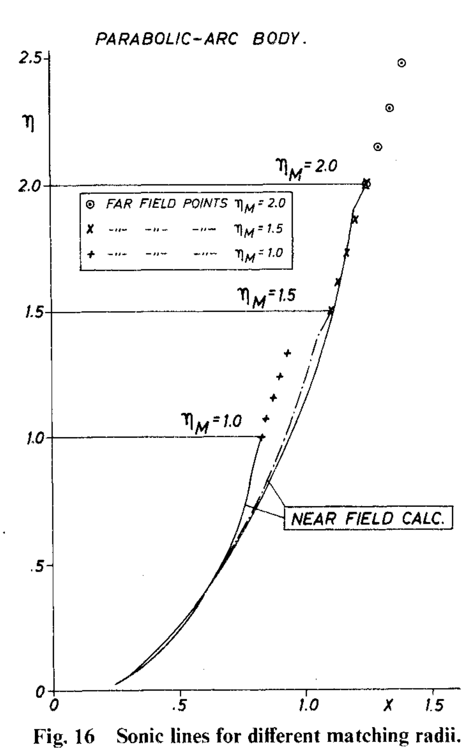

Fig. 16 Sonic lines for different matching radii.

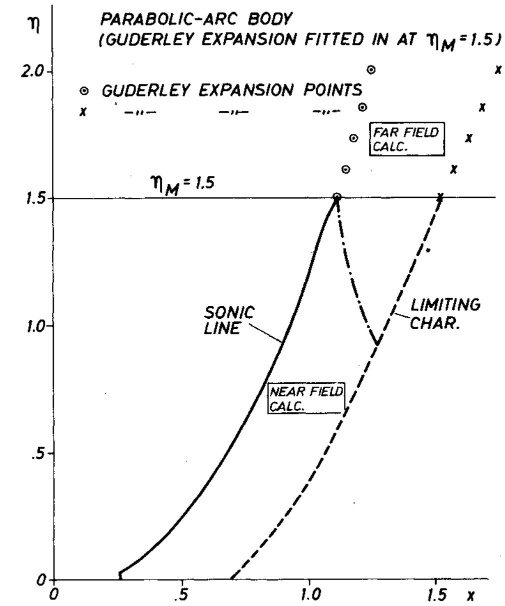

Fig. 17 Sonic line and limiting characteristic.

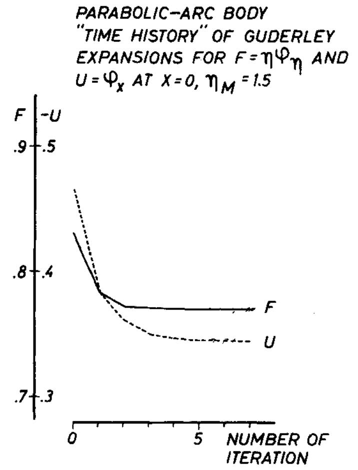

Fig. 19 Rate of convergence, free air case.

However, as the lateral disturbance pattern in transonic flow is of a very delicate nature, it is recommended to use a sonic far-field. A smaller number of terms used in the far-field expansion will cut the computer time considerably.

same sonic line close to the body. This property close to the body, which is rather independent of changes in the outer matching radius, is also demonstrated in Fig. 18. This concerns the velocity distribution $U(\eta)$ along $x = 0$. It is interesting to note that U tends to a finite value at $x = 0$, $\eta = 0$. The classical slender body approximation, Eq. (4), states a constant value of U at $x = 0$, a fact which is not realized in Fig. 18.

A closer look at Figs. 16 and 18 reveals a slight discontinuity between inner and outer solutions. The present experience then suggests either to use a modified Guderley expansion including second-order perturbations or to extend the matching radii to values where first-order perturbations of the basic solution, Eq. (8), are sufficient. Euvrard[18] has pointed out how higher-order terms can be accounted for. The relatively small deviations in Fig. 7 between the body pressure distributions obtained with the present method and the calculations made by Murman[13,14] at Mach number 0.999 seem to indicate that the body pressure is comparatively insensitive to the applied far-field. The author's experience has verified this observation in a number of cases.

C. The Rate of Convergence

The present reciprocating integration method converges rapidly and the experiences gained so far indicate 5–10 full cycle iterations for a typical free air case and 10–20 cycles for a typical wind-tunnel case. Figure 19 illustrates some convergence properties of a parabolic arc body in free air, while Fig. 20 shows a tunnel case with the same body. The number of mesh points in free air have been (25×60) for x and η respectively, while (29×40) points were used in the tunnel case.

The computer program for free air runs about 6 min of CPU-time for a typical case on an IBM 360/75 computer. The main part of this time is spent on the complicated far-field, which is repeatedly evaluated during each cycle to correct the parameters C and x_o. By changing to a CDC 6600 computer the CPU-time would probably be cut to about 1.5–2.0 min.

As a comparison it should be mentioned that a typical subsonic case, which was computed recently, needed about 13 sec on a CDC 6600. This program used backward-differencing in the supersonic domain and included Murman's[18] shock point operator, which seemed to speed up the convergence locally

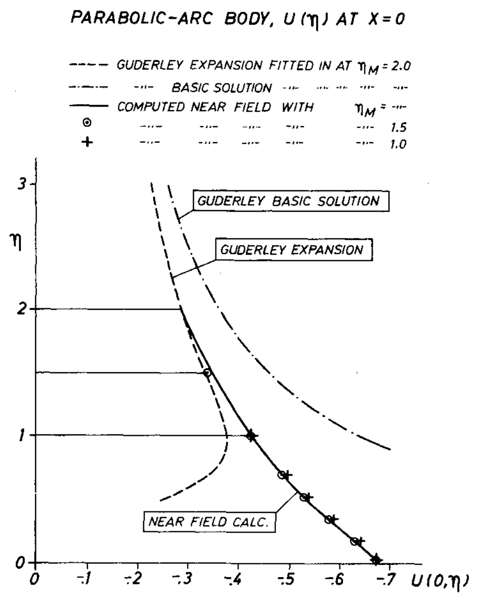

Fig. 18 Velocity distribution $U(\eta)$ for different matching radii, plotted along $x = 0$.

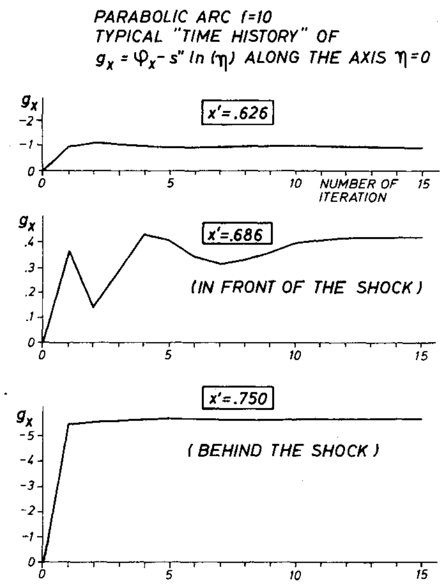

Fig. 20 Rate of convergence, wall interference case.

around the shock. The wind-tunnel case has been calculated on a small time-sharing computer and a comparison with a larger computer is difficult to make.

V. Conclusions

The present integration technique has proved to be a fast and reliable tool for computing axisymmetric sonic flow. The rate of convergence is high. The agreement with experiment and other methods of computation is found to be very good. The method is capable of producing shock-wave phenomena by using backward differences in the supersonic flow. Porous wind-tunnel walls can be treated by the method.

The method was recently applied to axisymmetric subsonic flows including embedded shock waves, and the results were equally good compared to sonic applications. The two-dimensional incompressible flow around a parabolic arc has also been calculated with an analog decomposition technique. The rate of convergence was here slightly slower but still rapid.

A nearby development of the method now is to try to extend its applications to three dimensions using conformal transformations in cross flow planes to generate new coordinate surfaces. Exploratory calculations have so far indicated encouraging results.

References

[1] Whitcomb, R. T., "A Study of the Zero-Lift Drag-Rise Characteristics of Wing-Body Combinations Near the Speed of Sound," Rept. 1273, 1956, NACA.

[2] Oswatitsch, K. and Keune, F., "Ein Äquivalenzsats für Nichtangestellte Flügel Kleiner Spannweite in Schallnaher Strömung," *Zeitschrift für Flugwissenchaften*, Vol. 3, No. 2, 1955.

[3] Cheng, H. K. and Hafez, M. M., "Equivalence Rule and Transonic Flows Involving Lift," USCAE Rept. 124, 1973, University of Southern California, Los Angeles, Calif.

[4] Berndt, S. B., "An Approach to the Problem of Axisymmetric Sonic Flow About a Slender Body," Proceedings of the 12th ICAM, Stanford University, edited by Hetenyi and Vincenti, Springer Verlag, Berlin, Germany, 1968.

[5] Guderley, K. G., "Axial Symmetric Flow Patterns at a Free Stream Mach Number Close to One," U.S. Air Force Technical Rept. 6285, Oct. 1950.

[6] Yoshihara, H., "On the Flow Over a Cone-Cylinder Body at Mach Number One," WADC Technical Rept. 52-295, 1952, Wright Air Force Development Center, Wright-Patterson Air Force Base, Ohio.

[7] Berndt, S. B. and Sedin, Y. C.-J., "A Numerical Method for Transonic Flow Fields," ICAS Paper 70-13, Sept. 1970.

[8] Guderley, K. G. and Yoshihara, H., "An Axial-Symmetric Transonic Flow Pattern," *Quarterly of Applied Mathematics*, Vol. 8, Jan. 1951, pp. 333.

[9] Randall, D. G., "Some Results in the Theory of Almost Axisymmetric Flow at Transonic Speed," *AIAA Journal*, Vol. 3, No. 12, Dec. 1965, pp. 2339.

[10] Murman, E. M. and Cole, J. D., "Calculation of Plane Steady Transonic Flows," *AIAA Journal*, Vol. 9, No. 1, Jan. 1971, pp. 114–121.

[11] McDevitt, J. B. and Taylor, R. A., "Pressure Distributions at Transonic Speeds for Slender Bodies Having Various Axial Locations of Maximum Diameter," TN 4280, July 1958, NACA.

[12] McDevitt, J. B. and Taylor, R. A., "Pressure Distributions at Transonic Speeds for Parabolic-Arc Bodies of Revolution Having Fineness Ratios of 10, 12, and 14," TN 4234, March 1958, NACA.

[13] Murman, E. M., private communication via letter from Murman to S. B. Berndt (Roy. Inst. of Tech., Stockholm), April 1971.

[14] Krupp, J. A. and Murman, E. M., "Computation of Transonic Flows Past Lifting Airfoils and Slender Bodies," *AIAA Journal*, Vol. 10, No. 7, July 1972, pp. 880–886.

[15] Spreiter, J. R. and Alksne, A. Y., "Slender-Body Theory Based on Approximate Solution of the Transonic Flow Equation," Rept. 2, 1959, NASA.

[16] Bailey, F. R., "The Numerical Calculation of Transonic Flow About Slender Bodies of Revolution," TND-6582, 1971, NASA.

[17] Euvrard, D. and Tournemine, G., "A Direct Method for Computing the Steady Flow at Mach Number One Past a Given Wing Air-Foil," *Proceedings of the 3rd International Conference on Numerical Methods in Fluid Mechanics*, in "*Lecture Notes in Physics*," Vol. 11, July 1972, edited by Cabannes and Teman, Springer-Verlag, Berlin, Germany.

[18] Euvrard, D., "Écoulement Transsonique à Grande Distance D'un Corps de Révolution," *Comptes Rendus Hebdomadaires des Seances de l'Academie de Sciences*, Paris, Vol. 260, pp. 5691, 1965.

[19] Murman, E. M., "Analysis of Embedded Shock Waves Calculated by Relaxation Methods," *AIAA Journal*, Vol. 12, No. 5, May 1974, pp. 626–633.